JOURNAL OF SOLID STATE CHEMISTRY 88, 443–450 (1990)

# High Temperature Gravimetric Study on Nonstoichiometry and Oxygen Adsorption of $SnO_2$

JUNICHIRO MIZUSAKI[1]

*Institute of Environmental Science and Technology, Yokohama National University, 156 Tokiwadai, Hodogaya-ku, Yokohama 240, Japan*

HIDEOMI KOINUMA

*Research Institute of Engineering Materials, Tokyo Institute of Technology, 4259 Nagatsuta, Midori-ku, Yokohama 227, Japan*

AND JUN-ICHI SHIMOYAMA,[2] MASASHI KAWASAKI, AND KAZUO FUEKI[3]

*Department of Industrial Chemistry, Faculty of Engineering, University of Tokyo, Hongo, Bunkyo-ku, Tokyo 113, Japan*

Received August 29, 1989; in revised form May 7, 1990

Gravimetric studies on porous $SnO_2$ between 200 and 1150°C and for oxygen partial pressures, $P(O_2)$, between 1 and $10^{-6}$ atm showed that the mass change of below 900°C is essentially due to oxygen adsorption on the $SnO_2$ surface. The oxygen adsorption was interpreted in terms of three Langmuir-type equations with different heats of adsorption. Mass changes due to nonstoichiometry were observed above 1000°C. The degree of nonstoichiometry of $SnO_2$ was found to be very small: For example, $d$ in $SnO_{2-d}$ at 0.1 atm of $P(O_2)$ was $7 = 10^{-5}$ at 1000°C and $2 \times 10^{-4}$ at 1150°C. The nonstoichiometry arises from oxygen deficiencies present as oxygen vacancies, $V_O^{\cdot\cdot}$; $d$ in $SnO_{2-d}$ above 1000°C is proportional to $P(O_2)^{-1/6}$. 

## 1. Introduction

Stannic oxide, $SnO_2$ exhibits high electrical conductivity (*1, 2*); its thin films are widely used for such purposes as transparent heating elements and transparent electrodes of solar cells and electrochromic displays. Because the conductivity of thin films or fine powders of $SnO_2$ is sensitive to environmental gases, many studies have been executed to utilize $SnO_2$ as chemical sensor materials (*3, 4*).

Bulk conduction of $SnO_2$ is *n*-type, which is attributed to oxygen deficiencies (*1, 2*), while changes in conductivity of thin films or powders in the presence of environmental gases are generally attributed to the adsorption of such gases on the surface (*3, 4*). Despite the large influence of nonstoichiometry

[1] To whom correspondence should be addressed.

[2] Present address: Asahi Glass Co., Ltd., Hazawa-cho, Kanagawa-ku, Yokohama 221, Japan.

[3] Present address: Department of Industrial Chemistry, Faculty of Science and Technology, Science University of Tokyo, Noda-shi, Chiba 278, Japan.



0022-4596/90 $3.00

and adsorption on the electrical conductivity, little work has been carried out to check the quantitative aspects of the nonstoichiometry and the oxygen adsorption of $SnO_2$.

In this work, we monitored the equilibrium mass of porous $SnO_2$ as functions of temperature and $P(O_2)$, and tried to determine separately the degree of bulk nonstoichiometry and the oxygen surface adsorption.

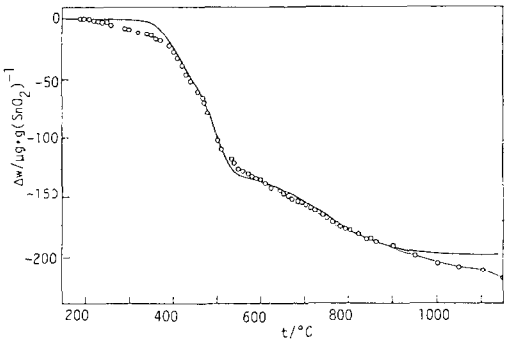


FIG. 1. The change in equilibrium weight of porous $SnO_2$ with temperature. $P(O_2)$: 0.138 atm. Surface area of the $SnO_2$ sample: 1.0 $m^2/g$. Heavy curve: calculated using Eq. (9) and the parameters of Table I.

## 2. Experimental

### *2.1. Samples*

Commercial $SnO_2$ powder (99.999% in purity) was pressed isostatically under a pressure of 1000 $kg/cm^2$. Then, the pressed samples were sintered at 1200°C for 2 hr in air so that they would not break during measurements. BET measurements, made by the courtesy of JGC Co, revealed that the surface area of the baked samples was 1.0 $m^2/g$.

### *2.2 Measurements*

An electric microbalance (Shimazu TG-31H), equipped with a reaction tube and a gas circulation and mixing system, was used for gravimetric measurements. Sample of 2–6 g was suspended in the reaction tube by a Pt wire from the microbalance. The reaction tube was placed in the electric furnace whose temperature was controlled within ±1°C. $Ar–O_2$ or $CO–CO_2$ gas mixtures of the desired ratios were prepared in the gas mixing system and introduced into the reaction tube at a total pressure of <0.2 atm.

Measurements were made both under isobaric conditions with stepwise changes in temperature, and under isothermal conditions with stepwise changes in the composition of environmental gas mixtures. For the isobaric measurements, correction was made for gas buoyancy effects. For gravimetry under isothermal conditions, the total pressure of the gas mixtures in the reaction tube was controlled to maintain gas mixtures of different $P(O_2)$ at the same density, i.e., the same buoyancy.

After correcting for buoyancy, the accuracy in gravimetric measurements was ±10 μg in the isobaric method and ±1 μg for the isothermal method.

## 3. Results and Discussion

### *3.1. Temperature and $P(O_2)$ Dependences of Equilibration*

*3.1.1. Results of gravimetry.* Figure 1 shows the equilibrium mass changes at temperatures above 200°C at a pressure $P(O_2)$ = 0.138 atm. A large weight loss is observed between 400 and 500°C. Above 500°C, the temperature coefficient of the weight loss gradually decreased with increasing temperature to an inflection point at near 1050°C. The temperature coefficient of the weight loss then rises with increasing temperature.

Figures 2 and 3 show the equilibrium mass changes as a function of $P(O_2)$ below 500°C

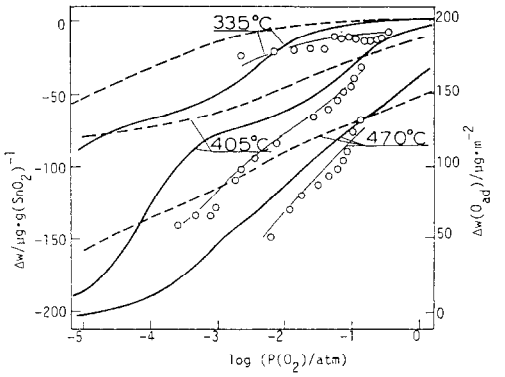


FIG. 2. The change in equilibrium weight of porous $SnO_2$ with $P(O_2)$ at temperatures below 500°C. Broken curves are calculated assuming that the oxygen adsorption processes of the types 1, 2, and 3 are expressed by Eq. (2). Heavy solid curves are calculated assuming the relationship of Eq. (3) holds for all of the three types of adsorption. The right-hand side scale indicates the amount of adsorbed oxygen.

and above 900°C, respectively. The mass changes with $P(O_2)$ at temperatures near 400–500°C are larger than those above 900°C.

*3.1.2. Separation of oxygen adsorption and oxygen nonstoichiometry.* We attempted to separate the observed mass loss caused by the desorption of surface oxygen from that due to evolution of bulk oxygen, based on reported conductivity (*1, 2*) and thermal expansion (*5*) data. We did not consider the effects of OH adsorption, because the data in Figs. 1–3 were obtained on samples kept for long times at high temperatures in the microbalance system in a controlled $O_2$–Ar environment.

According to Samson and Fonstad (*1*), the bulk conductivity of $SnO_2$ at temperatures above around 1000°C is proportional to $P(O_2)^{-1/6}$. Maier and Göpel (*2*) observed a $P(O_2)^{-1/6}$ dependence of conductivity above 800°C.

The $P(O_2)^{-1/6}$ conductivity dependence suggests that the number of conduction electrons, $n$, is related to the oxygen vacancy concentration, $[V_O^{\cdot\cdot}]$ due to nonstoichiometry by $n = 2[V_O^{\cdot\cdot}]$. (In this paper, we employ the Kröger–Vink notation (*6*) for defects.)

Below 800°C, Samson and Fonstad (*1*) found that the electrical conductivity is independent of $P(O_2)$, while Maier and Göpel (*2*) reported that the conductivity varies as $P(O_2)^{-1/4}$. According to Samson and Fonstad (*1*), the impurities are fully ionized; electroneutrality is maintained between the concentration of electrons, $n$, and that of impurity-donor ions (shallow donor level). In the model adopted by Maier and Göpel (*2*), electroneutrality is maintained between the concentration of impurities and of $[V_O^{\cdot\cdot}]$ (deep donor level). Thus, the conductivity at low temperatures is controlled by the concentration of different-valence impurities, because deviations from stoichiometric composition are smaller than the concentrations of impurities.

Sakurai and Takizawa studied the thermal expansion of $SnO_2$ by the use of high temperature XRD technique (*5*). It was shown that the thermal expansion coefficient increases with temperature above 800°C. They also concluded that the formation of oxygen vacancy becomes noticeable at temperatures above 800°C.

As shown in Fig. 1, the changes in mass of $SnO_2$ are larger below 1000°C than above 1000°C. In view of the $P(O_2)$ dependence of conductivity (*1, 2*) and the thermal expansion data (*5*), the large mass change between 200 and 1000°C in Fig. 1 is probably due to the change in the amount of adsorbed oxygen.

In the following sections, we discuss first the oxygen adsorption and, then, the oxygen nonstoichiometry of $SnO_2$.

### *3.2. Oxygen Adsorption on $SnO_2$*

*3.2.1. Temperature dependence.* The ratio, $\Delta w/\Delta T$, was calculated from Fig. 1 for $\Delta T = 20$°C, and is shown in Fig. 4 as a

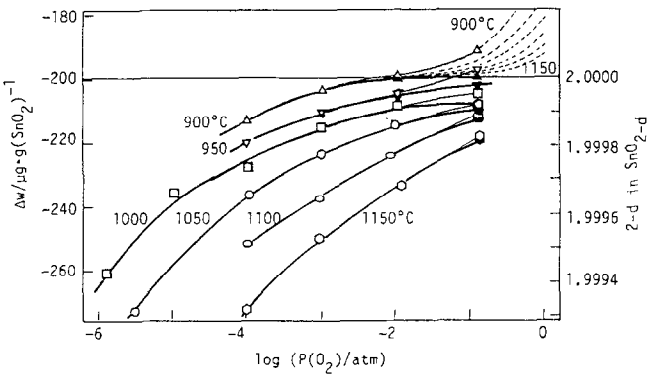


FIG. 3. The change in equilibrium mass of $SnO_2$ with $P(O_2)$ above 900°C. The right-hand scale shows the oxygen content in $SnO_2$. Broken curves show the mass change due to oxygen adsorption, calculated using Eqs. (6) and (9) with $m = 1$ and the parameters on Table I. Heavy curves show the mass change due to oxygen nonstoichiometry, obtained from the observed mass (symbols and thin curves) and the calculated mass change due to oxygen adsorption (broken curves).

function of temperature. These results are similar to the TPD chromatograms (*7*). However, the temperature of the desorption maximum is lower in the present work, presumably because the present $\Delta w/\Delta T$ data were determined under equilibrium conditions, while the TPD data includes kinetic effects: In the TPD measurements, the rate of oxygen desorption is recorded which is caused by departures from thermal equilibrium. If the surface desorption reaction is slow, the desorption peaks of the TPD chromatogram tend to shift to higher temperatures.

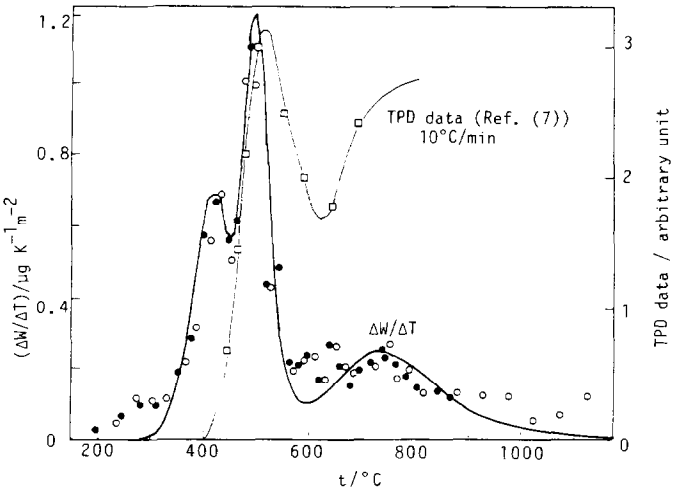


FIG. 4. The ratio, $(\Delta w/\Delta T)$, as a function of $T$. The heavy curve was calculated using Eq. (10) and the parameters are given in Table I. Thin curve is a typical TPD result cited from Ref. (*7*).

*3.2.2. Amount of oxygen adsorption to a surface tin atom.* According to Fig. 1, the oxygen released by the temperature change from 200 to 1000°C is 199.8 $\mu$g/g ($SnO_2$). For a BET surface area of $10^4$ $cm^2/g$, the mass of released oxygen corresponds to $7.516 \times 10^{14}$ atom O/$cm^2$.

For polycrystalline powder samples, it is difficult to determine which of the crystallographic surface of $SnO_2$ adsorbed how many oxygen atoms. Therefore we assume in the first approximation that the $SnO_2$ powder was spherical. In this case, the number of surface tin atoms for the molar volume of $SnO_2$ of 21.84 $cm^3$ is $9.125 \times 10^{14}$ atom Sn/$cm^2$. The amount of released oxygen relative to this value is 0.82. The oxygen adsorption is thus almost one monolayer.

*3.2.3. Equations for the fitting of the Langmuir-type adsorption model to the adsorption curve.* In Fig. 4, the $\Delta w/\Delta T$ vs $T$ plot exhibits three large peaks at 420, 490, and 735°C, respectively, with minima at 450 and 560°C. These peaks may correspond to three types of oxygen adsorption with different heat of adsorption.

Because the oxygen adsorption is monolayer, we assume the applicability of Langmuir-type adsorption isotherms for each of the three types of oxygen adsorption. That is,

$$w_i/w_{O_i} = k_i P(O_2)^m/\{1 + k_i P(O_2)^m\}, \quad (1)$$

where $w_i$ is the mass change due to oxygen adsorption and $w_{O_i}$ is the expected total mass change due to the oxygen adsorption of type $i$; $m = 1/2$ for an oxygen adsorption process according to the relation

$$1/2O_2 + V(ad)_i = O(ad)_i \quad (2)$$

and $m = 1$ for an adsorption process as expressed by

$$O_2 + V(ad)_i = O_2(ad)_i; \quad (3)$$

$k_i$ is the equilibrium constant for the adsorption of type $i$ expressed by Eq. (2) or (3).

Assuming an Arrhenius-type temperature dependence for $k_i$, we have

$$k_i = k_{O_i} \exp(-h_i/RT), \quad (4)$$

where $k_{O_i}$ is a constant. For isobaric conditions, using Eq. (4), Eq. (1) can be expressed as

$$w_i/w_{O_i} = K_i \exp(-h_i/RT)/\{1 + K_i \exp(-h_i/RT)\}, \quad (5)$$

where $K_i$ is given by

$$K_i = k_{O_i} P(O_2)^m. \quad (6)$$

From Eq. (5), we obtain

$$\partial w_i/\partial T = w_{O_i} h_i K_i \exp(-h_i/RT)/RT^2\{1 + K_i \exp(-h_i/RT)\}^2 = h_i(w_i w_{O_i} - w_i^2/RT^2 w_{O_i}). \quad (7)$$

In what follows, we designated the adsorption maxima at 420, 490, and 735°C as type 1, type 2, and type 3, respectively.

From Fig. 1, the mass changes between 200 and 450°C, 450 and 560°C, and 560 and 1000°C are essentially the same: The amount of adsorbed oxygen corresponding to each peak in Fig. 4 is essentially equivalent. Since the sum of the three types of adsorbed oxygen is 199.8 $\mu$g/g ($SnO_2$),

$$w_O = w_{O_1} = w_{O_2} = w_{O_3} = 66.6\ \mu g/g\ (SnO_2). \quad (8)$$

The mass of adsorbed oxygen $w$ at any temperature is given by

$$w = \sum_{i=1}^{3} w_i = w_O \sum_{i=1}^{3} K_i \exp(-h_i/RT)/\{1 + K_i \exp(-h_i/RT)\} \quad (9)$$

and $\partial w/\partial T$ is

$$\partial w/\partial T = \sum_{i=1}^{3} \partial w_i/\partial T = w_O \sum_{i=1}^{3} h_i K_i \exp(-h_i/RT)/RT^2\{1 + K_i \exp(-h_i/RT)\}^2. \quad (10)$$

TABLE I

FITTING PARAMETERS FOR THE TEMPERATURE DEPENDENCE OF OXYGEN ADSORPTION ON $SnO_2$

| $i$ | Estimated $(dw_i/dT)_{max}$ $10^{-6}$ gK$^{-1}$ | Estimated $T$ for $(dw_i/dT)_{max}$ °C | $h_i$ kcal mole$^{-1}$ | $K_i$ |
|---|---|---|---|---|
| 1 | −0.69 | 415 | −38.15 | $8.75 \times 10^{-13}$ |
| 2 | −1.10 | 500 | −77.07 | $1.75 \times 10^{-22}$ |
| 3 | −0.26 | 735 | −30.62 | $2.98 \times 10^{-7}$ |

*3.2.4 Fitting to the temperature change of the weight.* Fitting of Eqs. (9) and (10) to the experimental results was made by a trial and error method. After nearly 20 iterations, the best fit curves were attained using the parameters given in Table I. The fitting curves are shown in Figs. 1 and 4 by heavy curves.

*3.2.5. Fitting to the $P(O_2)$ dependence of adsorption curve.* The $P(O_2)$ dependence of oxygen adsorption at any temperature can be calculated from $h_i$ and $K_i$ values on Table I by using Eqs. (6) and (9). There are $2^3 = 8$ cases to be calculated, namely two cases, $m = 1/2$ and 1, for the adsorption equilibrium of each of the three types, $i = 1$, 2, and 3.

We calculated the $w$ vs log $P(O_2)$ relationship for each case at temperatures 335, 405, and 470°C and compared these with the experimental results in Fig. 2. In Fig. 2, the calculated relationships of two limiting cases are shown. The broken curves indicate the calculated results when the adsorption is expressed by Eq. (2), and the heavy solid curves show the results when Eq. (3) holds for any of the three types of adsorption. The calculations are closest to the experimental results when all the adsorption processes are assumed to be expressed by Eq. (3).

*3.2.6. Discussion on the fitting parameters.* Equation (3) shows that the distribution of adsorbed oxygen atoms on $SnO_2$ surface is paired rather than random, although this does not directly imply the formation of surface $O_2$ molecules. If the oxygen adsorption sites are paired and the surface diffusion of oxygen atoms to the next vacant pair sites is energetically hindered, the $O_2$ gas attached on the surface may occupy one pair vacant sites, and the adsorption equation is also described by Eq. (3).

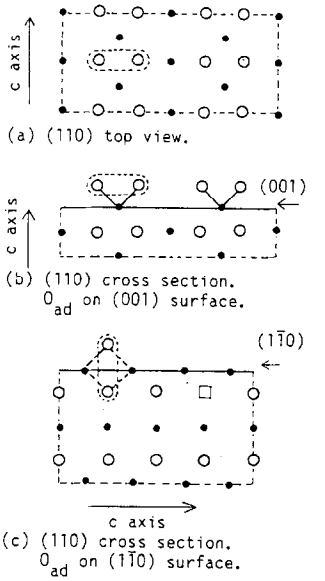


FIG. 5. The arrangements of tin and oxygen in and at the surface of $SnO_2$. In $SnO_2$, every two oxygen atoms (as indicated by surrounding dashes) tend to form pairs of atoms.

Such pairing of oxygen atoms in $SnO_2$ is displayed for the (110) plane as shown in Fig. 5a. Each neighboring oxygen atom in $SnO_2$ is closer to two Sn atoms along the $c$-axis than to Sn atoms along the 110 direction.

As shown in Table I, the heat of adsorption is 38 kcal/mole $O_2$ (19 kcal/mole O) for type 1, 77 kcal/mole $O_2$ (39 kcal/mole O) for type 2, and 30 kcal/mole $O_2$ (15 kcal/mole O) for type 3. $K_i$, which corresponds to the frequency factor, is the smallest for type 2 and the largest for type 3.

Presently, the nature for each type of adsorption mechanism is not clear. However, data for thermal decomposition of com-

pound gases on single crystalline $SnO_2$ (*8*) suggested that more than two types of adsorption still exist on a well-defined surface of single crystals. Hence, the three types of adsorption observed in this work is not necessarily attributed to adsorption on different crystallographic surfaces. Rather, such differences may be attributed to differences in the adsorption site, such as different coordinations to Sn atoms.

Some examples of different surface-oxygen coordination are shown in Fig. 5. In Fig. 5b, the adsorbed oxygen atoms are coordinated to one surface Sn atoms, and in Fig. 5c the pair sites stand perpendicular to the surface: one of the oxygen atoms in pair sites is below the surface Sn layer and another atom is on the surface.

### *3.3. Oxygen Nonstoichiometry of $SnO_2$*

*3.3.1. Determination of the stoichiometric point, $d = 0$.* The calculated oxygen nonstoichiometry is shown in Fig. 3 by the heavy curves and the right-hand side scale. In the figure, the thin broken curves show the mass changes with $P(O_2)$ at respective temperatures due to oxygen adsorption calculated with the parameters shown in Table I and Eqs. (5) and (6) with $m = 1$. From the difference in the calculated mass changes due to oxygen adsorption and the observed mass changes, the $d$ values in $SnO_{2-d}$ (heavy curves) are calculated. The oxygen content, $2 - d$, thus determined is shown on the right-hand side scale.

As shown in Fig. 3, the calculated $d$ value is always positive. That is, the oxygen nonstoichiometry in $SnO_{2-d}$ is of the oxygen-deficient type, as already suggested in earlier work (*1, 2, 5*).

*3.3.2. Defect model.* The oxygen partial molar enthalpy, $h_O$, in $SnO_{2-d}$ is given by

$$h_O = (R/2)\{\partial \ln P(O_2)/\partial(1//T)\}_d. \quad (11)$$

According to Eq. (11), $h_O$ can be obtained from the slope of a ln $P(O_2)$ vs $1/T$ plot.

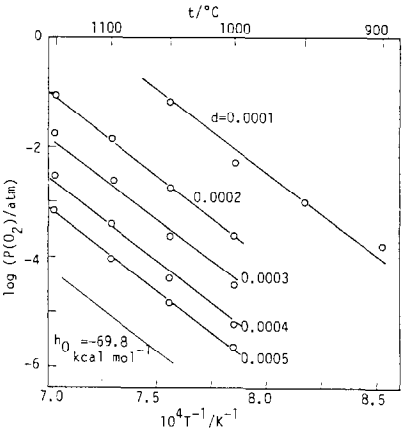


FIG. 6. Plot for the determination of the partial molar enthalpy of oxygen in $SnO_{2-d}$ with $d$ as a parameter.

Figure 6 shows the log $P(O_2)$ vs $1/T$ plot for $SnO_{2-d}$ with different $d$ values. The plots form straight lines and the slopes are essentially the same irrespective of $d$. In the region of $d$ and $T$ in Fig. 6, $h_O$ of $SnO_{2-d}$ is independent of $d$ and $T$. Therefore, the ideal solution approximation holds for the defect equilibrium in $SnO_{2-d}$ for the $d$ values observed in this work. $h_O$ is calculated to be $-69.8$ kcal/mole.

Figure 7 shows the plot of log $d$ as a function of log $P(O_2)$. The plot essentially obeys

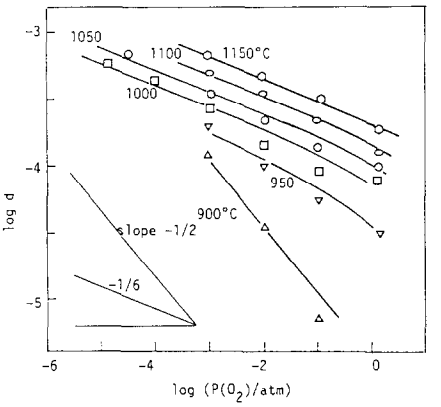


FIG. 7. $P(O_2)$ dependence of $d$ in $SnO_{2-d}$.

the $P(O_2)^{-1/6}$ law. For oxygen-deficient $SnO_2$, two types of ionic defects can be considered as the predominant defects. One is the interstitial Sn and another is the oxygen vacancy.

If the ideal solution approximation holds and the interstitial Sn, $Sn_i^{\cdot\cdot\cdot\cdot}$, predominates, the equilibrium with atmosphere is given by

$$SnO_2 = Sn_i^{\cdot\cdot\cdot\cdot} + O_2(g) + 4e \quad (12)$$

$$K = [Sn_i^{\cdot\cdot\cdot\cdot}]P(O_2)n^4, \quad (13)$$

where $K$ is the equilibrium constant and $n$ is the concentration of electrons. The electroneutrality condition is given by

$$4[Sn_i^{\cdot\cdot\cdot\cdot}] = n. \quad (14)$$

From Eqs. (13) and (14), we have

$$[Sn_i^{\cdot\cdot\cdot\cdot}] = n/4 = 4^{-4/5}K^{1/5}P(O_2)^{-1/5}. \quad (15)$$

As indicated by Eq. (15), when interstitial Sn predominates, both the conductivity and nonstoichiometry $d$ should obey the $P(O_2)^{-1/5}$ law.

When oxygen defects, $V_O^{\cdot\cdot}$, predominate, the equilibrium with the atmosphere is represented by

$$1/2O_2 + V_O^{\cdot\cdot} + 2e = O_O^x \quad (16)$$

$$K^{-1} = P(O_2)^{1/2}[V_O^{\cdot\cdot}]n^2a(O_O^x), \quad (17)$$

where $a(O_O^x)$ is the activity of lattice oxygen ions. The electroneutrality condition is expressed by

$$2[V_O^{\cdot\cdot}] = n. \quad (18)$$

From Eqs. (17) and (18), we have

$$[V_O^{\cdot\cdot}] = n/2 = 1/2(2K^{-1}a(O_O^x))^{1/3}P(O_2)^{-1/6}. \quad (19)$$

For small $d$, $[O_O^x]$ is close to 2; therefore, $a(O_O^x)$ is essentially constant. If the oxygen vacancy is the predominant ionic defect, the oxygen nonstoichiometry and electronic conductivity are proportional to $P(O_2)^{-1/6}$.

Since both the $d$ values observed in this work and the reported conductivity [1, 2] are proportional to $P(O_2)^{-1/6}$, it is confirmed that the predominant defect in $SnO_2$ consists of oxygen vacancies. The defect equilibrium in $SnO_2$ is expressed by Eqs. (16)–(18).

## 4. Conclusion

By the gravimetric measurements of porous $SnO_2$ as a function of $T$ and $P(O_2)$, the amount of adsorbed surface oxygen, and the oxygen nonstoichiometry of $SnO_2$, were separately determined.

The adsorption of oxygen on porous $SnO_2$ can be described by the sum of three types of Langmuir adsorption equation with different heats of adsorption. Surface oxygen is completely desorbed above 900°C.

The nonstoichiometry of $SnO_{2-d}$ is oxygen-deficient type with $V_O^{\cdot\cdot}$ formation, which is very small and is observable above about 1000°C. In $O_2$ gas at a pressure of $10^{-1}$ atm, $d$ is $7 \times 10^{-5}$ at 1000°C and $2 \times 10^{-4}$ at 1150°C. $[V_O^{\cdot\cdot}]$ $(= d)$ is proportional to $P(O_2)^{-1/6}$.

## Acknowledgments

The authors acknowledge Professor Hiroaki Tagawa of Yokohama National University for helpful discussion in the analysis of the adsorption data and Dr. Hideyuki Matsumoto and his co-workers of JGC Co. for the BET measurements of samples. This work is partly supported by Grant-in-Aid 62850142 for Developmental Scientific Research by Japan Ministry of Education.

## References

1. S. Samson and C. G. Fonstad, *J. Appl. Phys.* **44,** 4618 (1973).
2. J. Maier and W. Göpel, *J. Solid State Chem.* **72,** 293 (1988); W. Göpel, K. Schierbaum, H.-D. Wiemhofer, and J. Maier, *Solid State Ionics* **32/33,** 440 (1989).
3. T. Seiyama, A. Kato, K. Fujiishi, and M. Nagatani, *Anal. Chem.* **34,** 102 (1962).
4. N. Yamazoe, Y. Kurokawa, and T. Seiyama, "Proc. First meeting on Chemical Sensors, Fukuoka, Japan," pp. 35–40 (1983).
5. T. Sakurai and T. Takizawa, *High Temp. High Pressures,* **3,** 325 (1971).
6. F. A. Kröger, "The Chemistry of Imperfect Crystals," Elsevier, Amsterdam (1974).
7. N. Yamazoe, J. Fuchigami, M. Kishikawa, and T. Seiyama, *Surf. Sci.* **86,** 335 (1979).
8. H. Jacobs, W. Mokwa, D. Kohl, and G. Heiland, *Vacuum* **33,** 869 (1983).